Resveratrol exerts beneficial effects on the growth and metabolism of Lactuca sativa L

RESVERATROL EXERTS BENEFICIAL EFFECTS ON THE GROWTH AND METABOLISM OF *Lactuca sativa*

Ana Luiza Santos Wagner[1], Fabrizio Araniti[2], Emy Luiza Ishii-Iwamoto[1*] and Maria Rosa Abenavoli[3*]

[1]Laboratory of Biological Oxidations, Department of Biochemistry, State University of Maringa, 87020900 Maringa, Brazil.
[2]Department of Agricultural and Environmental Sciences (DISAA), University of Milan, Via Celoria, 2, 20133 Milan, Italy
[3]Department of Agriculture, University of Reggio di Calabria, Reggio Calabria, Italy.

[*]Corresponding author:
Maria Rosa Abenavoli, Phone: +39 0965-196-4350; e-mail: mrabenavoli@unirc.it
Emy Luiza Ishii-Iwamoto, Phone: 55-44-3011-4896; e-mail: eliiwamoto@uem.br

17 ABSTRACT

18

19

INTRODUCTION

Resveratrol (3,5,4′-trihydroxystilbene) is a phenolic micronutrient naturally found in a few plant species, including grapes, berries, peanuts, and pines (Harikumar and Aggarwal, 2008; Shishodia and Aggarwal, 2006). Over the last 50 years, the resveratrol research has increased due to its promising human health benefits such as the antioxidant, anticarcinogenic, antibacterial, anti-inflammatory, cardio- and neuroprotective properties (Vestergaard and Ingmer et al., 2019; Salehi et al., 2018; Shi et al., 2014; Belchi-Navarro et al., 2012). The mechanism underlying these beneficial effects was its ability to activate sirtuin-like protein deacetylases, redox-sensing enzymes involved in modulating metabolism regulation, stress responses, ageing processes, and longevity (Gertz et al., 2012; Halls and Yu, 2008).

In plants, resveratrol plays a crucial role in plant response to biotic and abiotic stress (Liu et al., 2019), such UV radiation and pathogens attacks (Vestergaard and Ingmer, 2019; Elshaer et al., 2018), boron toxicity (Sarafi et al., 2017), ozone (Grimmig et al., 2002) and saline stress (Kostopoulou et al., 2014). In particular, under stress conditions, plants trigger a complex biochemical system to increase the resveratrol synthesis and accumulation to confer protection (Vestergaard and Ingmer, 2019; Elshaer et al., 2018; Ahuja et al., 2012; Dednarek and Osbourn, 2009; Hammerschimidt, 1999). Some authors suggested that this protection was due to its ability to scavenge diverse reactive oxygen species (ROS), thereby increasing the cellular defense system by oxidative stress (Truong et al., 2018; Chang et al., 2009). King et al. (2006) demonstrated that resveratrol reduced the cell membranes damage maintaining their stability and limiting ROS stress in transgenic plants. Moreover, in tomato plants, the resveratrol accumulation caused an increase in ascorbic acid, glutathione, and antioxidant enzymes, which limited ROS damages (D'Intronio et al., 2009).

The beneficial resveratrol effects, as a potential natural crop protector, were also achieved by its exogenous application (Sarafi et al., 2017; Pociecha et al., 2014). In particular, Pociecha et al. (2014) observed that the resveratrol applied on wheat leaves, infected by powdery mildew, increased the phenolics metabolism and photosynthetic efficiency, reducing the damage during pathogenesis. Furthermore, the resveratrol application to peanut plants, before UV-C treatment, mitigated the damage symptoms of rusty spots and leaf wilt (Tang et al., 2010) and also delayed the decay process during apple fruit storage (Urena et al., 2003).

For all these reasons, researchers are focused on transgenic plants production in which the resveratrol synthase gene was overexpressed (Delaunois et al., 2009). The *sts* overexpression in tobacco, rice, apple and grape increased resveratrol content conferring higher resistence to abiotic and biotic stress (Chu et al., 2017; Dai et al., 2015; Zheng et al., 2015). For example, in transgenic rice seedlings, the resveratrol content was significantly increased (5–8 fold) under UV-C exposure compared to those grown under normal conditions (Zheng et al., 2015).

Alongside these benefits, resveratrol seems to inhibit weed growth. Recently, Mantovanelli et al. (2020) studied the effect of exogenous resveratrol application on seed germination, seedling growth, and mitochondrial energy metabolism in the crop/weed system, maize/ *Ipomea grandifolia*. They demonstrated that resveratrol stimulated maize seedlings growth, inhibiting, at the same concentration, the weed *I. grandifolia*, confirming its potential as crop protector.

Despite the stimulatory activity excercted by resveratrol has been largely demonstrated, limited knowledge are available on its effects on plant metabolism.

In this respect, the present study aimed to evaluate the effect of resveratrol on lettuce growth and development through a physiological and metabolomic approach to deeply insight into the mechanisms underlying its action.

MATERIALS AND METHODS

Dose-response curves

Lactuca sativa L. (var. Parris Island COS) seeds were sterilized with 2.0% sodium hypochlorite solution for 10 min and washed in distilled water. Then, 15 sterilized seeds were sown in square Petri dishes (100 x 100 mm) containing a double layer of filter paper, moistened with 6 ml of sterile deionized water (control) and acqueous solution of resveratrol (6.25, 12.5, 25, 50, 100, 200 and 400 µM) and transferred into a ventilated climatic chamber with 16/8 h (light/dark) photoperiod, 25±1℃ temperature, 120 µmol m^{-2} s^{-1} light intensity provided by a cold white fluorescent lamp (Polylux XL FT8, 55 W 8440) and 55% relative humidity for 6 days.

After the treatments, roots and aerial parts were collected, and their fresh weight (FW) was evaluated separately, and root length was measured. Plant material was then oven-dried for one week at 60℃ in order to determine the dry weight (DW). The average of aerial part FW in response to each resveratrol concentration allowed us to

Commentato [HC1]: X Ana: Please include the date of germination analysis and the following sentence: Then, the germinated seeds were counted using any extrusion of the radicle as a criterion,
and the total germination index (GT %) as described by Chiapusio et al. (1997) was calculated. The seedling were then treated for 6 days and roots and aerial parts werre collected…..Need to be correctly described!!

87 determine the ED_{50} (dose causing 50% stimulation of the total response), which was
88 then used for all the physiological and metabolic experiments.
89
90 *Leaf osmotic potential [Ψ (π)]*
91 After 6 days of treatment, leaf Ψπ was measured on four treated (100 μM) and
92 non-treated (0 μM) leaves according to Araniti et al. (2016). Treated and untreated
93 leaves were collected and frozen at -20℃. After 24 h, leaves were squeezed into a
94 syringe (the first drop was thrown away to avoid broken cells fluid contamination), the
95 extract was collected, and the Ψπ was measured with a cryoscopic osmometer
96 (Osmomat 030, Gonatec). The Ψπ leaf was expressed in mega pascal (MPA).
97
98 *In situ semi-quantitative determination of H_2O_2 and O_2^-*
99 Hydrogen peroxide was determined based on Araniti et al. (2016) with some
100 modifications. After 100 μM resveratrol treatment for 6 days, four fully expanded
101 treated (100 μM) and non-treated (0 μM) leaves were cut, vacuum infiltrated for 5 min
102 in 3,3'-diaminobenzidine (DAB) (1 mg ml^{-1}) solution (pH 3.8), and incubated for 8 h in
103 the same solution in the dark. After the incubation period, leaves were illuminated for 1
104 h and rinsed twice in pure ethanol to remove the pigments. Bleached leaves were stored
105 in 80% glycerol.
106 For O_2^- determination, four fully expanded treated (100 μM) and untreated (0
107 μM) leaves were vacuum infiltrated for 5 min with a 0.65 mg ml^{-1} solution of sodium
108 azide (NaN_3) in potassium phosphate buffer (pH 7.8) containing 0.1% of nitroblue
109 tetrazolium (NBT) (Halliwell and Gutteridge, 1985) and incubated in darkness for 20
110 min in the same solution. After the incubation, leaves were illuminated until the
111 appearance of stains. For both H_2O_2 and O_2^-, stained areas were determined by image
112 analysis with the software Image ProPlus v.6.0 (Media Cybernetics Inc., Bethesda, MD,
113 USA).
114
115 *Chlorophyll a fluorescence parameters*
116 The chlorophyll *a* fluorescence in treated (100 μM) and untreated (0 μM)
117 lettuce seedlings was monitored at the end of the treatment (6d), using the Maxi-
118 Imaging-PAM Chlorophyll Fluorescence System fluorometer (Walz, Effeltrich,
119 Germany), as previously described by Araniti et al. (2017c). The maximum efficiency
120 of photosystem II (PSII) in dark-adapted state (F_v/F_m), the effective PSII photochemical

quantum yield (ϕ_{II}), the quantum yield of regulated (ϕ_{NPQ}) and no-regulated no-photochemical energy loss in PSII (ϕ_{NO}), the no-photochemical quenching coefficient (q_N); the fraction of open PSII reaction centers based on a lake model (q_L) were evaluated. The photosynthetic response was monitored for 5 min, and fifteen measurements were obtained for each parameter at each measuring time.

Stomatal density and size

Immediately, after leaf detaching, both stomatal density (number of stomata per unit leaf area) and size (length between the junctions of the guard cells at each end of the stomata and width between the distal side of the guard cells) were evaluated on untreated and treated plants using an epifluorescence microscope system (Olympus bx53) used in bright field and expressed as a percentage compared to the control (Malone et al., 1993; Xu and Zhou, 2008). It should be specified that stomatal length might indicate the maximum potential opening of the stomatal pore, but not the aperture that actually occurs.

Samples extraction, derivatization, and analytical conditions

To evaluate the impact of resveratrol on plant metabolism, untreated (0 µM) and treated (100 µM) leaves were collected after 6 d, and the metabolome was extracted and derivatized as previously described by Lisec et al. (2006).

One µl of the derivatized extract was injected into a GC-MS apparatus (Thermo Scientific) equipped with a MEGA S.r.l. 5MS capillary column (30 m×0.25 mm×0.25µm) equipped with 10 m of pre-column. Injector and source were settled at 250 °C and 260 °C temperatures, respectively. Samples were injected in splitless mode with helium as a carrier gas with a flow of 1 ml/min. They were then analyzed using the programmed temperature proposed by Landi et al. (2020): isothermal 5 min at 70 °C followed by a 5 °C/ min ramp to 350 °C and a final 5 min heating at 330 °C. Mass spectra were recorded in electronic impact (EI) mode at 70 eV, scanning at 40–600 m/z range and scanning time 0.2 s. The mass spectrometric solvent delay was settled as 7 min. *n*-Alkane standards (C10–C40 all even) and blank solvents were injected at scheduled intervals for instrumental performance, tentative identification, and monitoring shifts in retention indices.

Analyses of GC-MS Metabolomics Data

Raw GC-MS data were analyzed using the software MS-DIAL ver. 4.48 coupled with a home built EI spectra libraries based on GOLM database, MassBank; Mass Bank of North America, etc. (Tsugawa et al., 2015; Tanaka et al., 2010; Kopka et al., 2005).

MS-DIAL analysis was settled as previously reported by Landi et al. (2020), and metabolite annotation was carried out comparing the retention index and the spectra similarity of the samples with those of the libraries, following the Metabolomics Standards Initiative (MSI) levels of the International Metabolomics Society: reported annotations were considered at level 2 (putative annotation based on spectral library similarity) or level 3 (putatively characterized compound class based on spectral similarity to known compounds of a chemical class) as suggested by Summer et al. (2007).

Experimental design and statistical analysis

All the experiments were carried out in a completely randomized design with N = 3 for dose-response curves, N = 5 for leaf osmotic potential, and N = 6 for chlorophyll *a* fluorescence parameters, leaf stomatal density, width and length, and metabolomic analysis.

Dose-response curves and physiological data were expressed as mean ± standard errors (SE) and were analyzed using analysis of variance (ANOVA) with Tukey's test as post-hoc ($P \leq 0.05$). The ED_{50} parameter was calculated, tightening the dose-response curve's raw data through a non-linear regression log-logistic equation model. The equation was chosen from those that had the highest determination coefficient (r^2) (*best fit*) (Software GraphPad Prism).

Metabolomic experiments were carried out using a completely randomized design with six replications for each treatment (N = 6). Metabolomic data were analysed using the software Metaboanalyst 5.0 (Chong and Xia, 2020). Metabolomics data were normalized using the internal standard (Ribitol 0.02 mg mL^{-1}) based normalization functions in the MS-DIAL software. The internal standard normalized dataset was transformed through "Log2 normalization," and Pareto scaled. The data were then classified through unsupervised multivariate Principal Component Analysis (PCA). The output comprised score plots to visualize the contrast between different samples and loading plots to explain the cluster separation. Metabolite variations were presented as a heatmap reporting only the *t*-test analysis's significant features (see below).

Partial Least-Squares discriminant analysis (PLS-DA) was used to highlight differences between the two treatments (0 and 100µM).

Data were then analysed through the univariate *t*-test ($P \leq 0.05$) to highlight statistical differences among single metabolites and treatment. A False Discovery Rate (FDR) was applied to the nominal *P*-values to control for false-positive findings.

Finally, to identify the metabolites coverage and the main altered pathways under resveratrol treatment, data were analysed using the Metaboanalyst enrichment analysis and pathway analysis tools.

199 RESULTS
200
201 *Germination and seedlings growth bioassays*
202 Resveratrol did not affect lettuce seed germination at all the concentrations
203 applied. Conversely, resveratrol treatment caused a strong stimulatory effect on *L.*
204 *sativa* growth, especially on the aerial part, where, at all concentrations (6.25-400 µM),
205 it significantly increased fresh biomass compared to the control (Fig. 1F). The raw data
206 obtained from the aerial part fresh biomass allowed us to estimate the ED_{50} equal to 100
207 µM (Fig. 1C). This concentration was used in all the subsequent experiments. The
208 highest resveratrol doses (100-400 µM) also significantly increased the dry biomass of
209 the aerial part (Fig. 1F)
210 Resveratrol treatment also increased the root fresh biomass at 25 and 200 µM
211 concentrations, while both root length (Fig. 1B) and dry weight (Fig. 1E) were not
212 affected by resveratrol.

Commentato [Fa2]: X Ana: We can't probably use the ED50 parameter, here there is a stimulatory effect. So, you can find the correct parameter, using GraphPAD prism software and explain it on mat and met

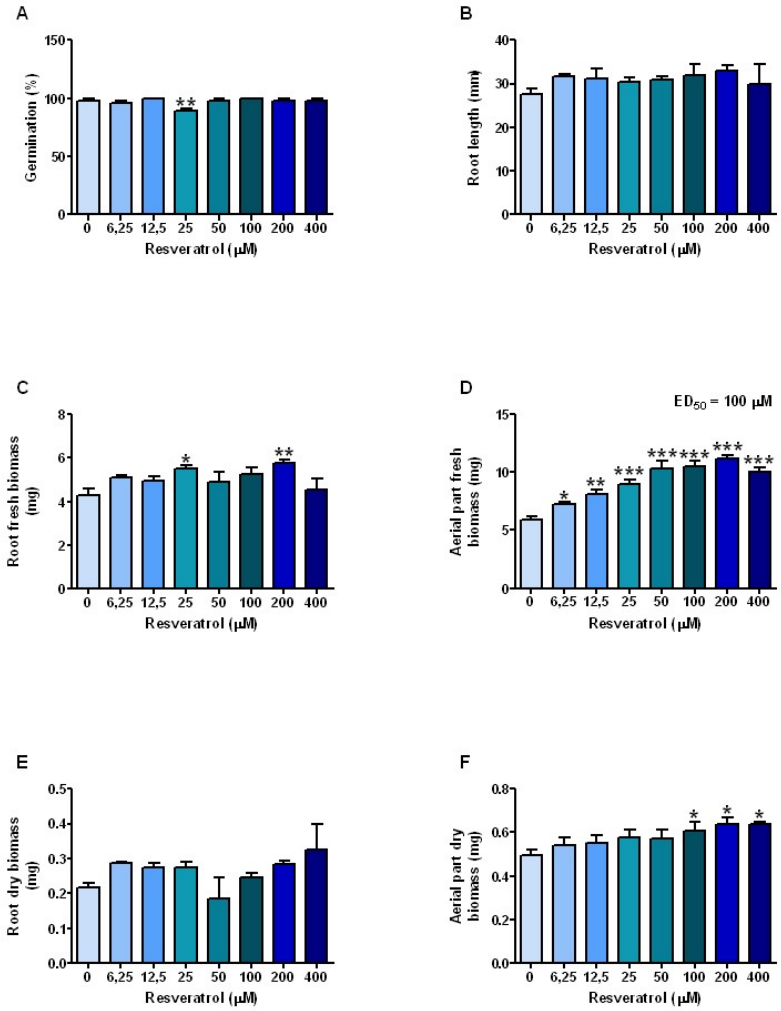

Figure 1. Dose–response curve of initial growth of *L. sativa* seedlings exposed to increasing doses of resveratrol: A) germination; B) root length; C) root fresh biomass; D) aerial part fresh biomass, E) root dry biomass, and F) aerial part dry biomass. ED_{50}: dose causing 50% stimulus of stem fresh biomass with respect to the control. Significant differences between means were identified by ANOVA with Tukey's test ($P \leq 0.05$). * ($P \leq 0.05$), ** ($P \leq 0.01$), *** ($P \leq 0.001$). N = 3.

In situ semi-quantitative determination of O_2^- and H_2O_2

As shown in Figure 2, leaves of control (Fig. 2A), and resveratrol (Fig. 2B) treated seedlings showed the same color and intensity, indicating that this potential elicitor did not alter the production of H_2O_2 in *L. sativa* leaves.

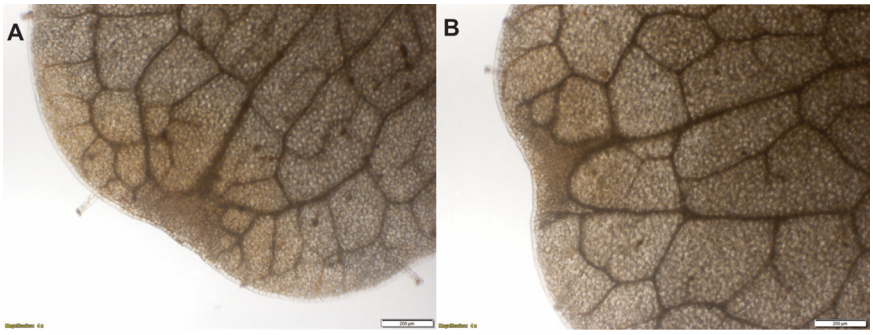

Figure 2. Semi-quantitative determination of H_2O_2 in *L. sativa* leaves treated with resveratrol 100 µM, showing the localization of the hydrogen peroxide on leaf surface after DAB staining: A) control leaf, and B) treated leaf. Image magnification 4X, scale bar 200 µm.

By contrast, resveratrol markedly reduced the superoxide production in *L. sativa* leaves. Indeed, treated leaves showed less and weaker color regions (Fig 3B) than the control (Fig 3A), supporting a reduction in the O_2^- production under resveratrol treatment.

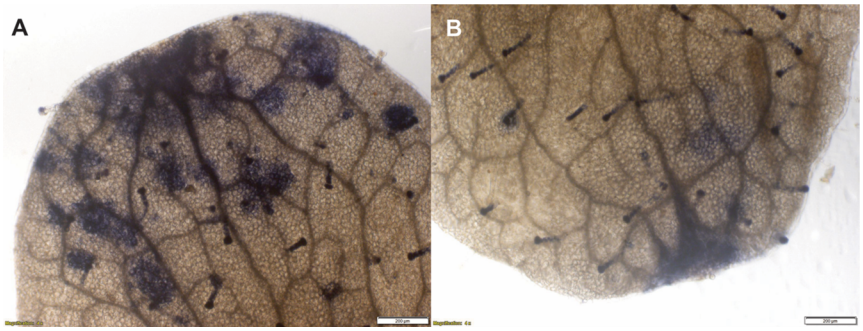

Figure 3. In situ O_2^- localization in resveratrol 100 µM treated and untreated *L. sativa* leaves, showing the localization of the superoxide on leaf surface after NBT staining: A) control leaf, B) treated leaf (Image magnification 4X, scale bar 200 µm).

Leaf stomatal density,size and width and leaf osmotic potential (Ψπ)

In both untreated and treated plants, stomata were open with turgid guard cells (Fig 4A and B). Resveratrol treatment did not alter stomatal density and length (Fig 4C and E), but increased stomatal width (Fig 4D).

Concerning leaf Ψπ, the data pointed out that resveratrol (100 µM) did not alter leaf osmotic potential of *L. sativa* compared to the control (Fig 5).

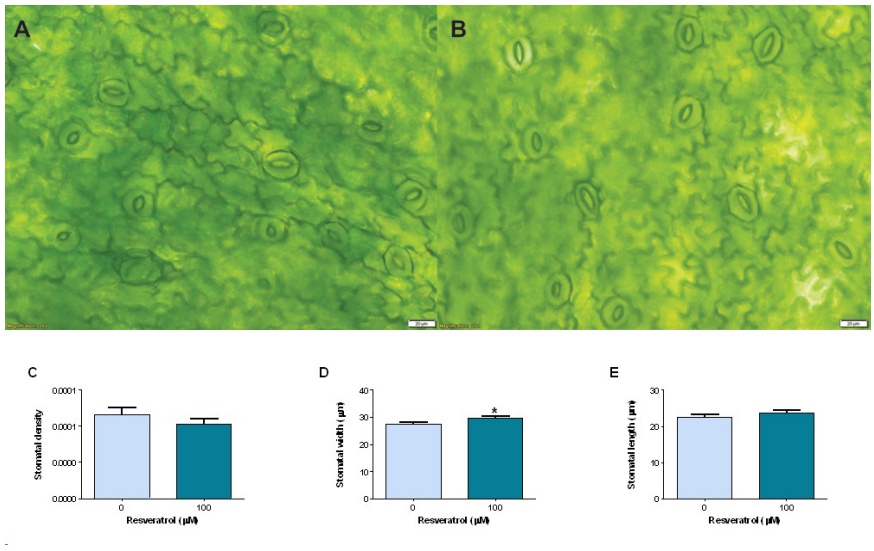

Figure 4. Micrograph of stomatal density of untreated (A) and treated (B) leaves of *L. sativa*.Stomatal density (C), width (D) and length (E) in treated and untreated leaves with 100 µM resveratrol Asterisks indicate significant differences between mean values (N = 6) of treated and control plants after *t*-test ($P \leq 0.05$): * ($P \leq 0.05$), ** ($P \leq 0.01$), *** ($P \leq 0.001$). Magnification 20X, scale bar 20 µm.

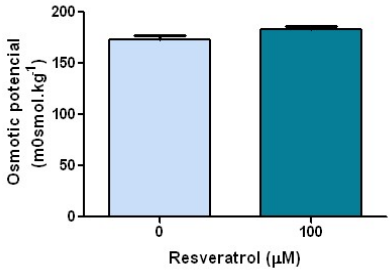

Figure 5. Effects of resveratrol 100 μM on the leaf osmotic potential [Ψ(π)] of *L. sativa*. Significant differences between means were identified by *t*-test ($P \leq 0.05$). N = 5.

Chlorophyll a fluorescence parameters

Among all the parameters, only Fv/Fm, the maximum quantum efficiency of dark-adapted PSII, was significantly increased by resveratrol treatment (Fig 6A), which did not alter the apparent electron transport rate (ETR), the effective PSII photochemical quantum yield (ϕ_{II}), the quantum yield of regulated (ϕ_{NPQ}) and the non-regulated energy emission in the form of fluorescence (ϕ_{NO}) (Fig 6B-E).

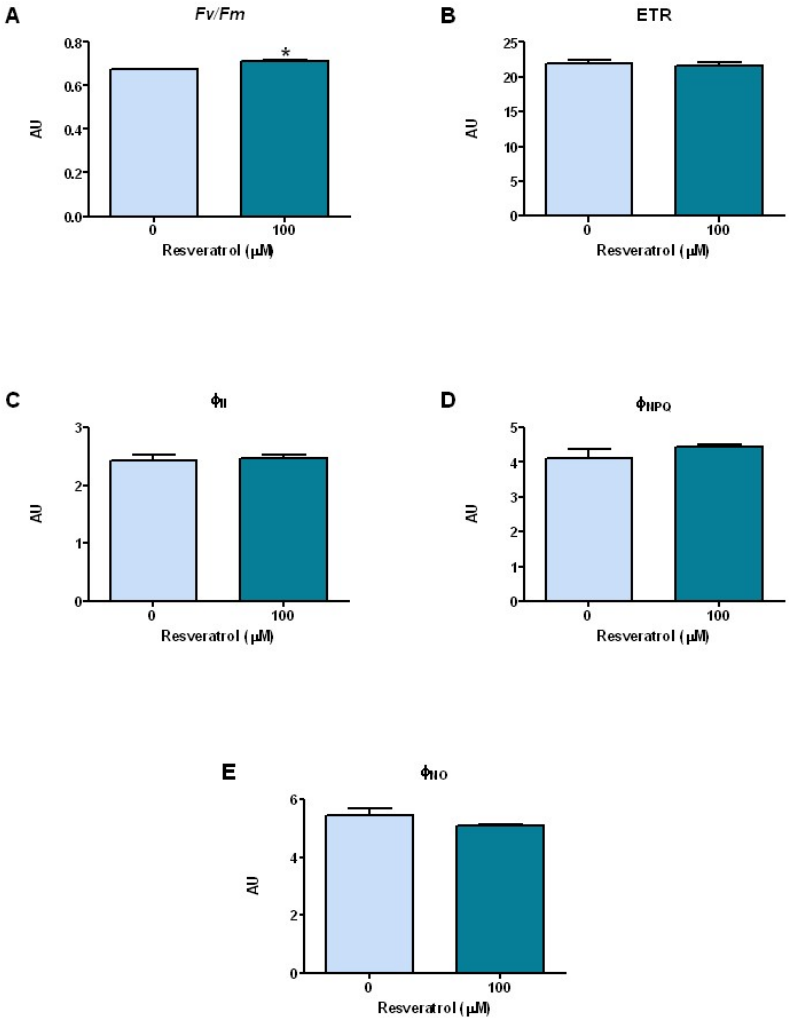

269
270

271

272 **Figure 6.** The maximum quantum efficiency of dark-adapted PSII (*Fv/Fm*) (A), the apparent electron
273 transport rate (ETR) (B), the effective PSII photochemical quantum yield (C) (ϕ_{II}), the quantum yield of
274 regulated emission of energy in the form of heat (ϕ_{NPQ}) (D), and the non-regulated emission of energy in
275 the form of fluorescence (ϕ_{NO}) (E) in the untreated and treated lettuce seedlings with resveratrol (100
276 µM). Significant differences between means were identified by *t*-test with $P \leq 0.05$: * ($P \leq 0.05$), ** ($P \leq$
277 0.01), *** ($P \leq 0.001$). AU = Arbitrary Units. N = 6.

278

Untargeted-Metabolomic analysis

The GC-MS-driven untargeted metabolomic analysis of resveratrol-treated seedlings allowed us to annotate and quantify 116 metabolites and extract 1005 unknown EI-MS shared features (Supplementary Table SXXX file excel).

Both annotated and unknown metabolites (Supplementary Table SXXX file excel), processed through MS-DIAL, were reported as supplementary data displaying their retention times, quantmass, signal/ noise ratio (S/N), RI similarity, total similarity, total spectrum similarity, and relative abundances.

A KEGG-based enrichment analysis (a method to identify classes of metabolites that are over-represented in a large set of metabolites and might have an association with treated seedlings phenotype) of the metabolic pathway revealed enrichment of galactose metabolism, amino sugar and nucleotide sugar metabolism, ascorbate and aldarate metabolism, among others (Figure 6a and Supplementary table SXXX). Most of these annotated metabolites belonged to the primary metabolism (amino acids, sugars, organic acids etc.) and in minor part to plant specialized metabolites (e.g., 2,3-Dihydroxybenzoate, quinic acid etc.).

The pathway analysis, which combines enrichment and topology analysis, pointed out that 28 pathways were significantly changed between the two treatments (Figure 6b and Supplementary table SXXX). Still, only 8 were characterized by an impact higher than 0.2 (starch and sucrose metabolism, alanine aspartate and glutamate metabolism, glycine serine and threonine metabolism, arginine biosynthesis, galactose metabolism, beta-alanine metabolism, glyoxylate and dicarboxylate metabolism, pantothenate and CoA biosynthesis) (Figure 6b and Supplementary table SXXXX).

The *t*-test analysis pointed out that 68 out of 116 metabolites were differentially produced between treatments. These metabolites mainly belonged to chemical classes of the amino acids (aspartic acid, glutamic acid, alanine, serine, among others), organic acids (tartaric acid, succinic acid, glyceric acid, among others), sugars and sugar alcohols (fructose, cellobiose, arabinose, galactinol, xylitol, among others), polyamines (putrescine and ornithine), etc., (Table 1).

Except for eleven metabolites (putrescine, DL-beta-hydroxybutyric acid, L-rhamnose, succinic acid, glyceric acid, glycerol-3-galactoside, creatinine, uridine, threonic acid, mannose and methylmalonic acid), all the statistically significant metabolites were stimulated by resveratrol treatment (Table 1).

The unsupervised Principal Component Analysis (PCA) was carried out on blank samples and all three samples group to demonstrate the system suitability. The PCA Score Plot, built on the first (PC1) and the second component (PC2), revealed clear discrimination of sample groups against blanks, highlighting model robustness (Supplementary Figure S1a). The components separated control and treated groups with no outliers (Supplementary Figure S1), indicating that the metabolomic analysis was reliable and could reflect the metabolic profile changes induced by the resveratrol treatment.

Both unsupervised PCA runs on MS-DIAL suggested that metabolites (Supplementary Figure S1b) and unknowns features (Supplementary Figure S1c) were useful to a clear sample groups' discrimination. Further, both unsupervised PCA analyses (Fig. 7a) and Supervised Partial Least Squares Discriminant Analysis (PLS-DA), carried out only on the annotated metabolites (Fig. 7b), demonstrated group separation with the first 2 principal components (PCs), explaining 72.2% variance for PCA and 71.5% variance in PLS-DA score plots. The PLS-DA model's robustness was validated by the permutation test, which highlighted a high R^2 and Q^2 for both latent variables (Supplementary Figure S2).

PLS-DA derived variable importance of projection (VIP) scores (built on the first 30 metabolites with a VIP score higher than 1.4) revealed melezitose, gallic acid, glutamine, and aspartic acid, among others, like the ones with the highest VIP scores between the two treatments (Fig. 7c).

Finally, the cluster analysis on the top of the heat map (reporting in a false scale color the variation of significantly different metabolite concentrations for each sample and replicate) further confirmed total discrimination between the two treatments, which clustered separately (Figure 7d).

a)

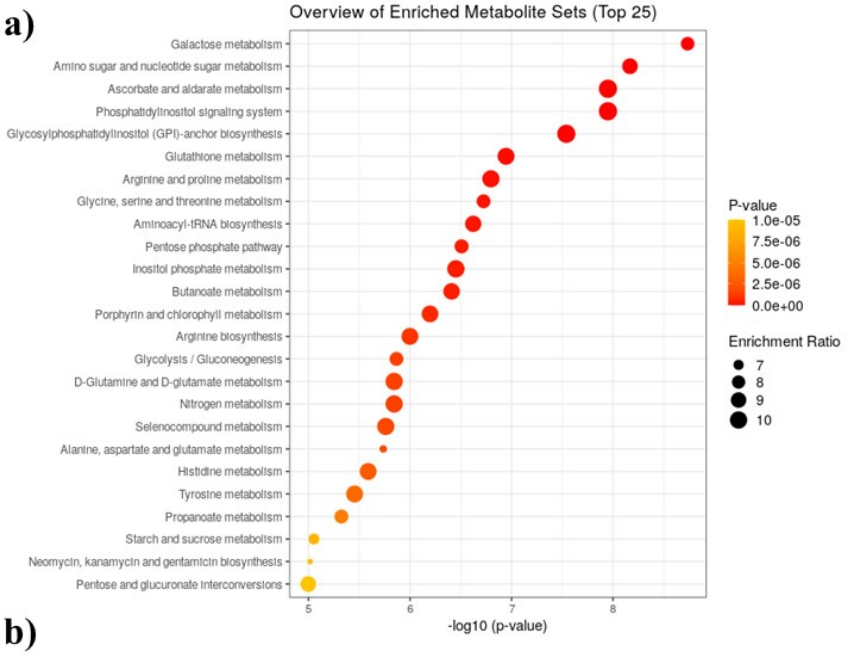

b)

	Total Cmpd	Hits	Raw p	-LOG10(p)	Holm adjust	FDR	Impact
Starch and sucrose metabolism	22	5	3.06E-05	4.5149	0.00068073	5.41E-05	0.63853
Alanine aspartate and glutamate metabolism	22	5	2.89E-07	6.5384	1.19E-05	2.22E-06	0.57914
Glycine serine and threonine metabolism	33	5	1.67E-06	5.7761	4.86E-05	4.20E-06	0.41558
Arginine biosynthesis	18	4	1.00E-06	5.9992	3.41E-05	3.54E-06	0.36117
Galactose metabolism	27	8	1.58E-07	6.801	6.80E-06	1.82E-06	0.25476
beta-Alanine metabolism	18	3	6.31E-05	4.2003	0.001072	9.67E-05	0.25397
Glyoxylate and dicarboxylate metabolism	29	7	1.51E-05	4.8217	0.00037688	3.15E-05	0.22451
Pantothenate and CoA biosynthesis	23	3	0.015483	1.8101	0.092898	0.017371	0.21166

Fig. 6: (a) Pathway enrichment analysis revealed different metabolic pathways enriched during resveratrol treatment (*P* value cut off ≤ 0.05). (b) Results from "Pathway Analysis" carried on the concentrations of metabolite identified in resveratrol treated and untreated seedlings. Total Cmpd: the total number of compounds in the pathway; Hits: the matched number from the uploaded data; Raw p is the original *P* value, -Log(*P*) value: the logarithm of the original *P*-value calculated from the enrichment analysis; Holm adjust: the Holm adjustment used to counteract the problem of multiple comparisons, FDR: the false discovery rate applied to the nominal *P*-values to control for false-positive findings; Impact: the pathway impact value calculated from the combination of enrichment and topology analysis.

Table 1: Metabolites differentially accumulated in the control and resveratrol-treated samples. Data were analyzed through Student's t-test ($P \leq 0.05$). A False Discovery Rate (FDR) was applied to the nominal *P*-values to control for false-positive findings. Negative values of the t-stat indicate a significant increase of the specific metabolite in resveratrol-treated seedlings. (N = 6).

Metabolites	t.stat	p.value	FDR	Class
Phosphate	-37.609	4.21E-12	4.76E-10	
Galactose	-30.953	2.91E-11	1.64E-09	Sugar
L-Arabinose	-29.163	5.24E-11	1.97E-09	Sugar
N-Acetyl-D-glucosamine	-27.628	8.95E-11	2.18E-09	
Putrescine	27.422	9.63E-11	2.18E-09	Polyamine
DL-beta-Hydroxybutyric acid	25.241	2.18E-10	4.11E-09	
Glucosaminic acid	-24.524	2.90E-10	4.68E-09	
Inositol	-16.876	1.12E-08	1.58E-07	Sugar alcohol
Sophorose	-16.15	1.72E-08	2.15E-07	Sugar
Lactitol	-15.483	2.58E-08	2.91E-07	Sugar alcohol
Uridine 5'-diphospho-N-acetylglucosamine	-15.304	2.88E-08	2.96E-07	
Xylose	-13.096	1.28E-07	1.20E-06	Sugar
Palatinitol	-12.85	1.53E-07	1.33E-06	Sugar alcohol
Melibiose	-12.685	1.73E-07	1.40E-06	Sugar
Gentiobiose	-12.547	1.92E-07	1.45E-06	Sugar
Maltitol	-12.149	2.60E-07	1.84E-06	Sugar alcohol
Lactobionic acid	-12.07	2.77E-07	1.84E-06	
Glucose 6-phosphate	-10.682	8.66E-07	5.43E-06	
L-Rhamnose	10.146	1.39E-06	7.55E-06	Sugar
Galactinol	-10.123	1.42E-06	7.55E-06	Sugar alcohol
L-Glutamic acid	-10.114	1.43E-06	7.55E-06	Amino acid
L-Ornithine	-10.033	1.54E-06	7.55E-06	Polyamine
Lactose	-10.017	1.57E-06	7.55E-06	Sugar
Succinic acid	9.9904	1.60E-06	7.55E-06	Organic acid
L-Alanine	-9.9057	1.73E-06	7.84E-06	Amino acid
Lactulose	-9.3589	2.91E-06	1.23E-05	Sugar
L-Iditol	-9.346	2.94E-06	1.23E-05	Sugar alcohol
4-Hydroxyphenylacetic acid	-9.1653	3.51E-06	1.42E-05	
Trehalose	-8.8309	4.91E-06	1.91E-05	Sugar
Glyceric acid	8.4732	7.09E-06	2.67E-05	Organic acid
Cellobiose	-7.9975	1.18E-05	4.30E-05	Sugar
2,3-Dihydroxybenzoate	-7.8281	1.42E-05	5.03E-05	
Glycerol-3-galactoside	7.3477	2.46E-05	8.42E-05	
L-Aspartic acid	-7.1904	2.96E-05	9.84E-05	Amino acid
Arabinose	-7.1229	3.21E-05	0.000103	Sugar
Lysine	-7.1036	3.28E-05	0.000103	Amino acid
DL-Allothreonine	-6.77	4.92E-05	0.00015	Amino acid
5-Keto-D-Gluconate	-6.518	6.74E-05	0.000197	

L-Norleucine	-6.5114	6.80E-05	0.000197	Amino acid
L-Isoleucine	-6.3214	8.67E-05	0.000239	Amino acid
dehydroascorbic acid	-6.2487	9.52E-05	0.000253	
Glutaric acid	-6.2388	9.65E-05	0.000253	Organic acid
Creatinine	6.1681	0.000106	0.000272	
Uridine	5.8723	0.000157	0.000394	
Tartrate	-5.821	0.000168	0.000413	Organic acid
Threonic acid	5.7757	0.000179	0.00043	Organic acid
L-Serine	-5.6616	0.000209	0.00049	Amino acid
1,6-Anhydro-beta-D-Glucose	-5.6503	0.000212	0.00049	
Methylamine	-5.5625	0.00024	0.000534	
Isomaltose	-5.5594	0.000241	0.000534	Sugar
Xylitol	-5.4559	0.000279	0.000605	Sugar alcohol
Xylonolactone	-5.1024	0.000462	0.000986	
meso-Erythritol	-4.3951	0.001345	0.002815	Sugar alcohol
Oxamic acid	-4.3671	0.001406	0.002888	Organic acid
L-Norvaline	-4.2893	0.001588	0.003204	Amino acid
L-Valine	-4.2538	0.001679	0.003329	Amino acid
Galactosamine	-4.2064	0.00181	0.003527	
Glycine	-3.866	0.003129	0.005994	Amino acid
Oxalic acid	-3.7346	0.003881	0.007309	Organic acid
Glycerol	-3.5777	0.005031	0.009319	Sugar alcohol
Mannose	3.5198	0.00554	0.010098	Sugar
Methylmalonic acid	3.474	0.005981	0.010728	Organic acid
Fructose	-3.0832	0.011578	0.020442	Sugar
Hexacosane	-2.9796	0.013818	0.024022	Alkane
N-acetylornithine	-2.9698	0.01405	0.024055	
DL-Pyroglutamic acid	-2.9538	0.014442	0.024357	
Cafferic acid	-2.9263	0.015137	0.025154	
3-Amino isobutyric acid	-2.7135	0.021801	0.035703	

356

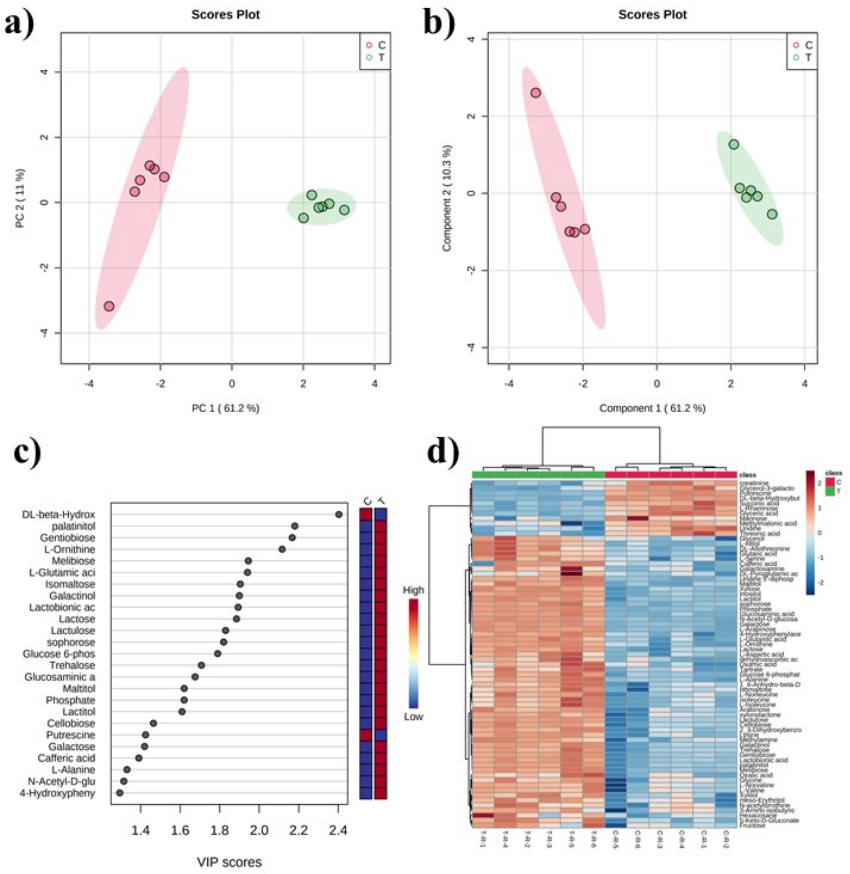

Fig. 8: (a) Principal component analysis (PCA) and (b) Partial least square discriminant analysis (PLS-DA) showing score plots discriminating the control (C), and resveratrol-treated (T) groups by virtue of the first 2 PCs. (c) PLSDA derived analysis variable importance of projection (VIP) features for the groups, and (d) overlay heat map of the significantly affected metabolites (selected by *t*-test with $P \leq 0.05$). Each square represents the different stage's effect on every metabolite's relative abundance using a false-colour scale. Colours dark red and blue indicate relative metabolite abundances, increased and decreased, respectively (n = 6).

370

371 DISCUSSION

372 Resveratrol is a stilbenoid compound produced by plants involved in plant defense
373 responses to abiotic and biotic stress (Chang et al., 2011; Hasan and Bae, 2017).
374 Although most studies had mainly focused on the potential antimicrobial, antibacterial
375 (Mattio et al., 2020) antioxidant activity in response to abiotic and biotic stress (Hasan
376 and Bae, 2017), few investigations have been carried out on resveratrol effect on plant
377 growth, regardless its role in the induction of the protective mechanisms (Bruno and
378 Sparapano, 2006; Li et al., 2019). Here we used *L. sativa*, a sensitive crop species to
379 natural and synthetic compounds (Macías et al. 2000) to study resveratrol effects on
380 germination and early seedlings growth. According to Mantovanelli et al. (2020),
381 resveratrol did not significantly affect the lettuce seed germination. Similar results were
382 also reported in radish seeds where resveratrol did not have intensive germination-
383 stimulating properties, unlike protectors to ethanol seed sterilization treatment (Balanov
384 et al., 2020). Conversely, it significantly stimulated fresh and dry biomass of the aerial
385 part of lettuce, already at low concentrations, leaving unchanged the length and biomass
386 of root system. This positive effect was already observed in maize seedlings, although
387 only at 440 µM resveratrol concentration (Mantovanelli et al. 2020). In particular, the
388 fresh weight biomass increased in a dose-dependent manner ranging from 6.25-400 µM.
389 By contrast, the positive effect on dry weight was observed at 100-400 µM range.
390 According to Mantovanelli et al. (2020), both primary root length and root fresh weight
391 were not affected by resveratrol, although a significant increase in root dry weight
392 biomass was observed at 200 µM resveratrol, confirming the trend already reported in
393 maize (Mantovanelli et al., 2020). However, these results appeared in contrast with
394 Fang et al. (2010), which observed an inhibitory effect of this phytoalexin on root
395 lettuce growth. The highest concentration adopted by these authors could justify this
396 contrasting response. Thereby, our results indicated that the aerial part could be
397 considered a main target of resveratrol; thus, we focused on a better understanding of
398 the resveratrol activity using the ED_{50} value. One hundred µM treatment confirmed the
399 beneficial effect of this elicitor on lettuce aerial part (stem and leaves) and its ability to
400 stimulate plant growth when exogenously applied (Pociecha et al., Mantovanelli et al.,
401 2021). Mantovanelli et al. (2020) hypothesized that resveratrol is structurally similar to
402 the synthetic oestrogen diethylstilbestrol, naturally produced by plants, which
403 stimulated plant growth, cell division and pollen germination (Janeczco et al., 2005).

404 They further suggested a behaviour similar to brassinosteroids, which induced plants
405 tolerance under stress conditions by increasing the antioxidant activity (Farriduddin et
406 al., 2013) and stimulated plant growth (Clouse and Sasse, 1998). Thus, we hypothesized
407 that the stimulatory effect of resveratrol on lettuce could be linked to its potent ROS
408 scavenger ability (Stojanovic et al., 2001). In plants, ROS, generated in several
409 organelles (Dietz et al., 2016; Huang et al., 2016), included hydroxyl radicals (˙OH) and
410 superoxide anions ($O^{\cdot-2}$), and molecular states, hydrogen peroxide (H_2O_2), and singlet
411 oxygen ($^1O_2$) (Apel and Hirt, 2004; Mittler et al., 2004). While ROS are important for
412 plant growth, performing many physiological processes (Elstner, 1987; Choudhury et
413 al., 2017), their overproduction, under various biotic and abiotic conditions, causes lipid
414 peroxidation, DNA and protein damage, resulting in perturbation of the cellular redox
415 state that can ultimately lead to oxidative stress and cell death (Gill and Tuteja, 2010;
416 Dumnod and Rivoal, 2019). Interestingly, 100 µM resveratrol reduced the $O^{\cdot-2}$
417 production, leaving unchanged the H_2O_2 content. In particular, the superoxide anion,
418 produced in chloroplasts, mitochondria, endoplasmic reticulum, and peroxisomes under
419 their normal metabolism (Sharma et al., 2012), is an unstable molecule (Juan et al.,
420 2021) rapidly converted to hydrogen peroxide, permeable to the membrane. Trans-
421 membrane NADP-oxidases (NOXs) and the mithocondrial and chloroplastic electron
422 transport chain (ETC) are the most important enzymes and organelles producing $O^{\cdot-2}$
423 and H_2O_2 (Fisher et al., 2006). However, it is not clear whether resveratrol acts directly
424 as anti-ROS, or indirectly by blocking ROS production by enzymes such as NADPH
425 oxidase (NOX) enzymes or by influencing the expression of cellular pro- and
426 antioxidants. The down-regulation of NOXs after resveratrol treatment to protect
427 mammalian cells from oxidative functional damages is strongly demonstrated (Block
428 and Gorin, 2012). Mantovanelli et al. (2021) demonstrated that at concentrations above
429 440 µM, resveratrol inhibited the respiration coupled to ADP phosphorylation and
430 NADH-oxidase, succinate-oxidase and ATP synthase activities in mitochondria isolated
431 from *Z. mays* roots, conferring a beneficial effect on plant growth.
432 The importance of the antioxidant network in maintaining high rates of photosynthesis
433 has been demonstrated in many studies (Foyer and Shigeoka, 2011) since ROS
434 overproduction and accumulation can also inhibit photosynthesis, limiting plant growth
435 and yield (Mittler and Blumwald, 2010). Thus, the maintenance of $O^{\cdot-2}$ low
436 concentration by resveratrol could induce a greater photosynthetic efficiency. For
437 example, by preserving ROS homeostasis, melatonin also helps to maintain a better

performance of the photosynthetic process under salinity stress (Yang et al., 2019). Furthermore, Pociecha et al. (2014) demonstrated that resveratrol stimulated photosynthetic efficiency during pathogenesis, influencing the energy flux parameter for electron transport and improving the stability and efficiency of membranes. Among Chlorophyll fluorescence (ChlF) parameters, the quantum efficiency of photostistem II (PSII) in dark- and light-adapted conditions (Fv/Fm and Fv'/Fm') are usually good indicators of photosynthetic activity, physiological function, as well as healthy and stress conditions, (Jia et al., 2019). In particular, Fv/Fm, which indicates the initial maximal efficiency of photons captured by open PSII reaction centers (Butler, 2008), is used as an indicator of health and plant growth (Feng et al., 2015) more than Fv'/Fm' (Jia et al., 2019). For example, under a range of nitrogen (N) fertilizer, the Fv/Fm increased along with N application (Liu et al., 2008). By contrast, a reduced value of Fv/Fm was indicative of the probable physical damage at the level of the complex antenna accompanied by a reduction in the PSII efficiency as observed under stress conditions such as drought (Maxwell and Johnson, 2000; Prieto et al., 2009). Interestingly, the results indicated that all the chlorophyll fluorescence parameters remained unchanged except for Fv/Fm whose ratio was higher in the resveratrol treated leaves, conferring a higher stability rate of the complex PSII/LHC and increasing lettuce growth. The resveratrol action on photosyntesis may also be associated with the stimulation of polyamines, which scavenge free radicals and activate some antioxidant enzyme activities, subsequently reducing oxidative damage (Liu et al. 2015) and are essential in the regulation of plant growth and development (Martin-Tanguy, 2001). In lettuce treated seedlings, a high level of L-ornithine, the precursor of polyamines, was reported. Anyway, resveratrol's protective effect on PSII is negligible toto consider it as a PSII enhancer.

On the other hand, resveratrol treatment did not affect stomatal density and size but induced a higher stomatal width, suggesting an increased gas exchange in treated plants. This phenomenon is commonly observed with natural compounds belonging to the classes of phenols. For example, An et al. (2016) demonstrated that the accumulation of flavonols in the guard cells, induced by an elicitor, is involved in ROS detoxification and the ABA-induced inhibition of stomatal closure. The stomatal width is an important indicator of the stomatal aperture being related to a higher rate of CO_2 exchange and photosynthetic efficiency. Therefore, the results suggest that resveratrol, more than

acting as a PSII protector and/or stimulating agent, could burst the metabolism, as also suggested by the metabolomic analysis.

Among the metabolic pathways, resveratrol significantly enriched the galactose metabolism and the ascorbate and aldarate metabolism (the third most enriched pathway). Both pathways are closely related to each other since the galactose pathway is involved in ascorbate biosynthesis (Smirnoff and Wheeler, 2000). Interestingly, besides the high accumulation of galactose observed in resveratrol-treated plants showed an accumulation of dehydroascorbic acid (DHA). It should not be excluded that the increase in DHA content could be due to the oxidation of AA during sample handling and analysis, meaning that treated plants were particularly rich in ascorbate content. In fact, it has been reported that AA is unstable in aqueous solutions under aerobic conditions (extraction and derivatization conditions) being converted in DHA (Levandoski et al., 1964; Dewhirst et al., 2018).

Among different pathways for ascorbate biosynthesis (Jain and Nessler, 2000; Agius et al., 2003; Lorence et al., 2004), the galactose is one of the most important pathway recently discovered. It is well known that high ascorbic acid content was positively correlated with high galactose level induced by a higher activity of L-galactose-1-phosphate phosphatase (GPP) in rice (Zhang et al., 2015), or L-galactose guanyltransferase, in *Arabidopsis* (Laing et al., 2007; Bulley et al., 2009) or Lgalactose DH, in tomato cultivars (Cervilla et al., 2007) or GPP and GME co-expression in *Nicotiana benthamiana* (Laing et al., 2015).

The alterations in galactose and starch and sucrose metabolism were generally underligned by a high accumulation of different classes of sugars including polyiols, which play a pivotal role in providing carbon and energy for normal functioning of cellular metabolism and in regulating growth and development of plants acting as signal molecules. The osmoprotectant roles of sugars (glucose, fructose, threalose etc.) and sugar alcohols (glycerol, inositol, maltitol etc), all stimulated by resveratrol treatment, have been widely accepted. They could regulate the osmotic adjustment and/or provide membrane protection and ROS scavenging activity under stress (Kerepesi and Galiba 2000; Murakeozy et al. 2003Murakeozy et al. 2003; Ahmad and Sharma 2008; Livingston et al. 2009; Van den Ende and Valluru 2009; Koyro et al. 2012). Among them, the trehalose should be mentioned in response to resveratrol treatment. . This molecule plays an important role either in optimal or under stress conditions, acting as

an osmoprotectant or osmolyte protecting membranes, proteins and decreasing aggregation of denatured proteins (Ashraf and Harris 2004; Koyro et al. 2012).

Furthermore, besides sugar accumulation, resveratrol-treated lettuce seedlings were characterized by an accumulation of several proteinogenic amino acids (glutamic acid, aspartic acid, alanine, among others), known to be involved either in osmoprotection or in protein biosynthesis and biomass production (Rai, 2002). The joint upregulation of the biochemical pathways involved in energetic and aminoacid metabolism could be the main reason for resveratrol-induced growth promotion.

.

References

An, Y., Feng, X., Liu, L., Xiong, L., & Wang, L. (2016). ALA-induced flavonols accumulation in guard cells is involved in scavenging H2O2 and inhibiting stomatal closure in Arabidopsis cotyledons. *Frontiers in plant science*, *7*, 1713.Smirnoff, N., & Wheeler, G. L. (2000). Ascorbic acid in plants: biosynthesis and function. *Critical reviews in plant sciences*, *19*(4), 267-290.

Rai, V. K. (2002). Role of amino acids in plant responses to stresses. *Biologia plantarum*, *45*(4), 481-487.

Foyer, C. H., & Mullineaux, P. M. (1998). The presence of dehydroascorbate and dehydroascorbate reductase in plant tissues. *FEBS letters*, *425*(3), 528-529.

Levandoski, N. G., Baker, E. M., & Canham, J. E. (1964). A monodehydro form of ascorbic acid in the autoxidation of ascorbic acid to dehydroascorbic acid. *Biochemistry*, *3*(10), 1465-1469.

Dewhirst, R. A., & Fry, S. C. (2018). The oxidation of dehydroascorbic acid and 2, 3-diketogulonate by distinct reactive oxygen species. *Biochemical Journal*, *475*(21), 3451-3470.

Malone, S. R., Mayeux, H. S., Johnson, H. B., & Polley, H. W. (1993). Stomatal density and aperture length in four plant species grown across a subambient CO2 gradient. *American Journal of Botany*, *80*(12), 1413-1418.

Xu, Z., & Zhou, G. (2008). Responses of leaf stomatal density to water status and its relationship with photosynthesis in a grass. *Journal of experimental botany*, *59*(12), 3317-3325.

Chang X, Heene E, Qiao F, Nick P. The phytoalexin resveratrol regulates the initiation of hypersensitive cell death in Vitis cell. PLoS One. 2011; 6: e26405. doi: 10.1371/journal.pone.0026405 PMID:22053190

Mattio L.M, Catinella G., Dallavalle S. and Pinto A. Stilbenoids: A Natural Arsenal against Bacterial Pathogens. Antibiotics 2020, 9, 336; doi:10.3390/antibiotics9060336

Hasan M., Bae H. An Overview of Stress-Induced Resveratrol Synthesis in Grapes: Perspectives for Resveratrol-Enriched Grape Products. Molecules. 2017. 14;22(2):294. doi: 10.3390/molecules22020294

ha formattato: Inglese (Regno Unito)

Formattato: SpazioDopo: 12 pt

Tingting Lia,b,1, Yuqi Lia,b,1, Zhijuan Sunc , Xiangli Xia,b, Guangli Shad 5 , Changqing Maa,b, Yike Tiana,b, Caihong Wanga,b, Xiaodong Zheng. Resveratrol alleviates the KCl salinity stress of *Malus* 1 *hupenensis* Rhed. seedlings by regulating K+/Na+ homeostasis, 2 osmotic adjustment, and Reactive Oxygen Species scavenging

~~D'Introno~~ D'Introno A, Paradiso A, Scoditti E, D0Amico L, de Paolis A, Carluccio MA, et al. Antioxidant and antiinflammatory properties of tomato fruits synthesizing different amounts of stilbenes. Plant Biotechnol J.2009; 7; 422–429. doi: 10.1111/j.1467-7652.2009.00409.x PMID: 19490505

Balanov P E, Smotraeva V , Abdullaeva M S, Fedorov A V, Ivanchenko O B, Volkov M P. Protective properties of resveratrol in biological systems containing ethanol 2ARM 2020 IOP Conf. Series: Earth and Environmental Science 640 (2021) 052029 IOP Publishing doi:10.1088/1755-1315/640/5/052029

ACKNOWLEDGEMENTS

This work was supported by grants from the Araucária Foundation (112/2010) do Estado do Paraná, National Council for Scientific and Technological Development (CNPq). Ana Luiza ~~Wagner Zampieri~~Santos Wagner fellowship holder from the Coordination for the Improvement of Higher Education Personnel (CAPES).

CONFLICT OF INTEREST: The authors declare that they have no conflict of interest.

ha formattato: Tipo di carattere: 12 pt, Inglese (Stati Uniti)

ha formattato: Inglese (Stati Uniti)

ha formattato: Tipo di carattere: (Predefinito) Times New Roman, 12 pt, Inglese (Stati Uniti)

ha formattato: Inglese (Stati Uniti)

ha formattato: Tipo di carattere: (Predefinito) Times New Roman, 12 pt, Inglese (Stati Uniti)

ha formattato: Inglese (Stati Uniti)

Formattato: Giustificato, Interlinea: singola

Formattato: Interlinea: singola

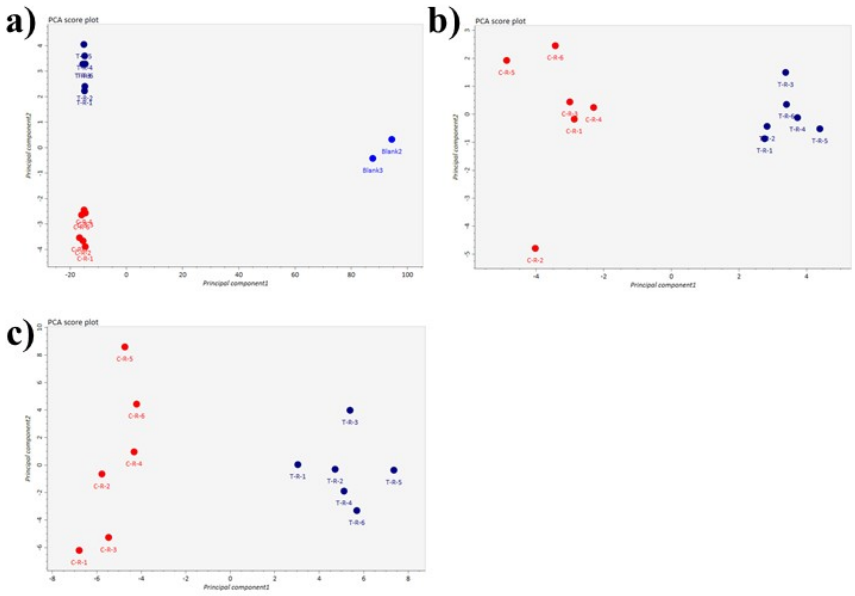

Fig. S1: a) compounds vs blank, b) known; c) unknown

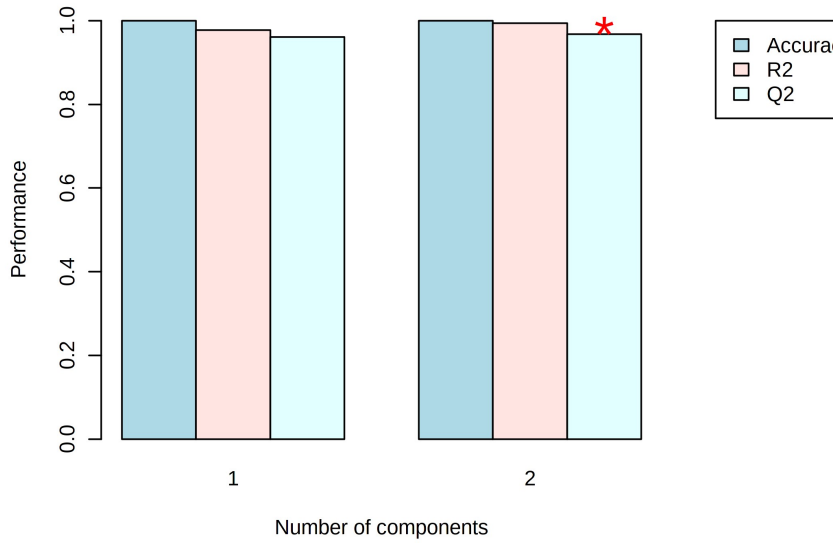

603

604 Fig. S2: PLS-DA model's robustness was validation